Pediatr Radiol (1999) 29: 238–243

Eu-Leong H. J. Teo
Peter J. Strouse
Martin R. Prince

Applications of magnetic resonance imaging and magnetic resonance angiography to evaluate the hepatic vasculature in the pediatric patient

Received: 4 May 1998
Accepted: 12 October 1998

E.-L. H. J. Teo[1] · P. J. Strouse · M. R. Prince
University of Michigan Health System,
Ann Arbor, MI 48109, USA

P. J. Strouse (✉)
Section of Pediatric Radiology,
C. S. Mott Children's Hospital,
University of Michigan Hospitals,
1500 Medical Center Drive, Ann Arbor,
Michigan 48109-0252, USA

Present address:
[1] Kandang Kerbau Women's and Children's Hospital, 100 Bukit Timah Road, Singapore 229899

Abstract Magnetic resonance imaging (MRI) and magnetic resonance angiography (MRA) offer several techniques to evaluate the hepatic vasculature. These techniques are briefly reviewed with reference to the pediatric population. Examples of MRI and MRA in the evaluation of the hepatic vasculature in pediatric patients are presented.

Introduction

Indications for the evaluation of the hepatic vasculature in the pediatric population are rapidly expanding. Although usually adequate, sonographic and Doppler evaluation of the hepatic vasculature is still operator-dependent and occasionally technically difficult. Conventional angiography, while being the gold standard, carries the risks of an invasive procedure and involves radiation exposure. Magnetic resonance imaging (MRI) and magnetic resonance angiography (MRA) are powerful alternatives for demonstrating the hepatic vasculature. In this essay we will summarize the MR techniques available and provide examples of their usefulness in pediatric patients.

Materials and methods

The exact MR protocol selected will vary, depending on the indication for the examination and size of the child being imaged. A body coil is used for teenagers, with a head coil used for smaller patients who fit into it. As a rule, thinner slices and smaller field of view are used in younger patients to define the anatomy better. The infant or young child usually requires sedation and will be unable to cooperate with breath-holding instructions. Fortunately, images obtained in quiet respiration suffice for most sequences [1]. In the occasional patient under general anesthesia, respiration can be temporarily suspended to optimize imaging.

At our institution, patients are imaged on a 1.5 Tesla magnet (Signa or Horizon, G. E. Medical Systems, Milwaukee, Wis.). T1- and T2-weighted sequences are frequently obtained to evaluate the hepatic parenchyma and hepatic masses. These sequences should not be overlooked as they are valuable contributors to assessing the hepatic vasculature. Three types of MRA sequences are available: time-of-flight, phase contrast and 3D gadolinium enhanced; however, phase contrast is now rarely used in evaluating the hepatic vasculature. The MRI and MRA sequences are complementary, as each utilizes a different property of magnetic resonance to form images.

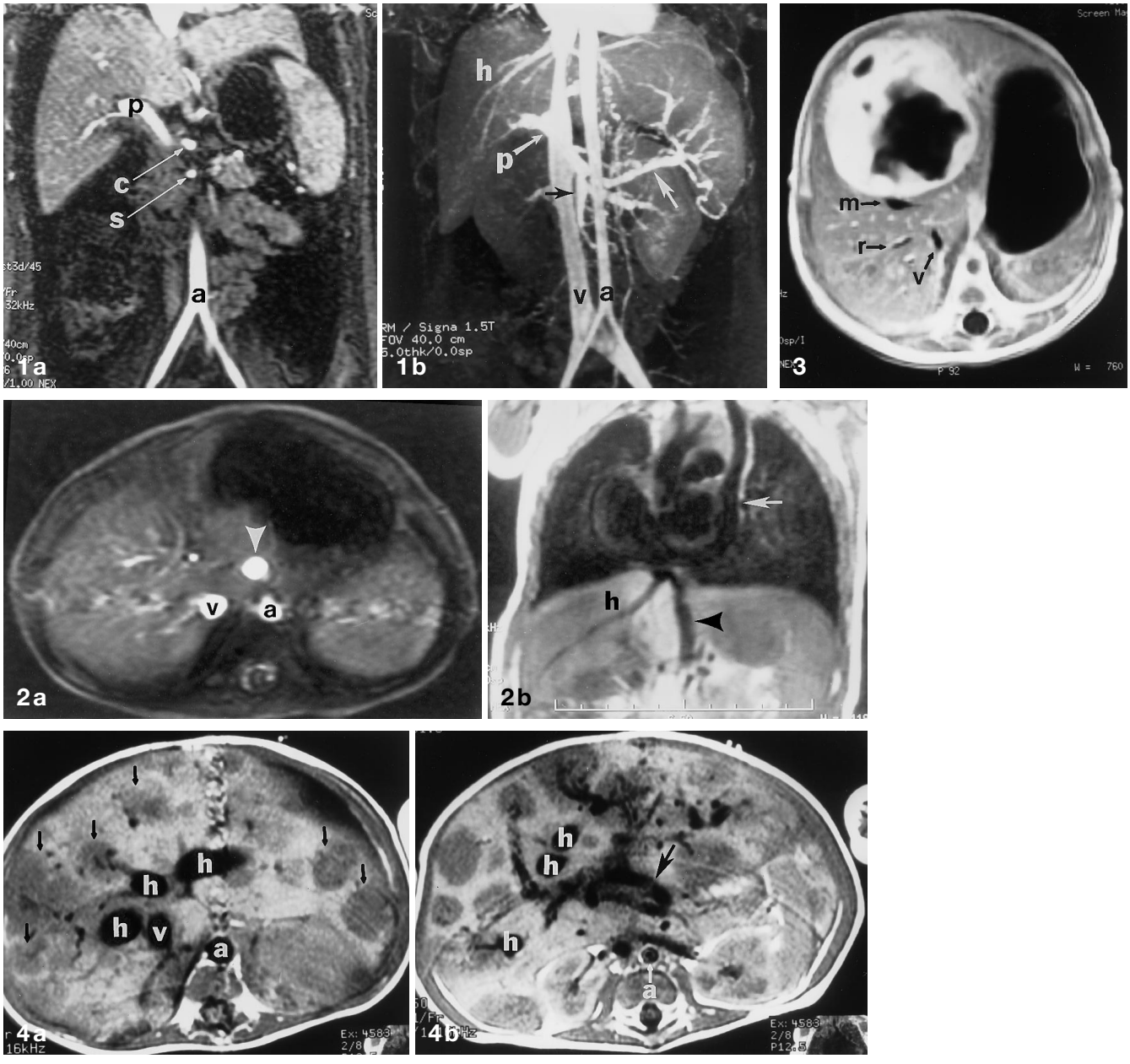

Fig. 1 Normal anatomy in a 17-year-old woman with fulminant liver failure due to Wilson's disease. **a** Coronal 3D Gd MRA source image during the arterial phase showing the main portal vein (*c* celiac axis, *s* superior mesenteric vein, *a* aorta). **b** Coronal MIP 3D Gd MRA image during the venous phase showing the main portal vein *(p),* superior mesenteric vein *(black arrow),* splenic vein *(white arrow),* hepatic veins *(h),* inferior vena cava *(v)* and the aorta *(a).* Images obtained during breath-holding

Fig. 2 Congenital absence of the portal vein in a 10-month-old infant in which ultrasound failed to demonstrate a normal portal vein. **a** Axial TOF image shows this anomalous vein *(arrowhead)* continuing upward and not entering the porta hepatis (*v* IVC, *a* aorta). **b** Coronal black blood T1-weighted image shows the anomalous vein *(arrowhead)* entering the right atrium (*h* hepatic vein, *white arrow* left superior vena cava draining to coronary sinus). Images obtained in quiet respiration with the infant sedated

Fig. 3 Focal hemangioendothelioma in a 4-day-old neonate. Gadolinium enhanced black blood T1-weighted image shows marked peripheral enhancement in a mass, which is located anterior to the middle hepatic vein *(m).* Other images demonstrated the left hepatic vein displaced leftward by the mass, confirming localization of the mass to be within the medial segment of the left lobe. Coronal images are also frequently helpful for tumor localization (*r* right hepatic vein, *v* IVC). Images were obtained during mechanical ventilation with the infant under general anesthesia

Fig. 4 Hemangioendotheliomatosis in a 3-month-old female. **a** Axial black blood T1-weighted image shows multiple low-signal intensity hemangioendotheliomas distributed throughout the liver *(arrows).* The hepatic veins *(h)* are enlarged, indicating increased flow due to arteriovenous shunting (*v* IVC, *a* aorta). **b** Axial black blood T1 image at a lower level shows the large caliber hepatic artery *(black arrow)* and small caliber infrahepatic aorta *(a)* (*h* Hepatic veins). Images obtained during mechanical ventilation in a previously intubated infant

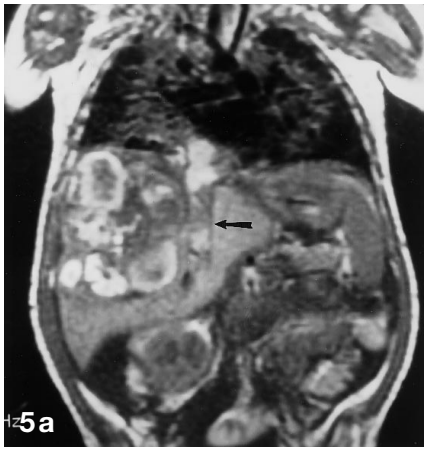

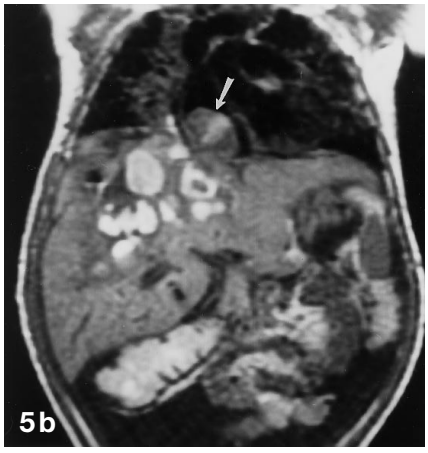

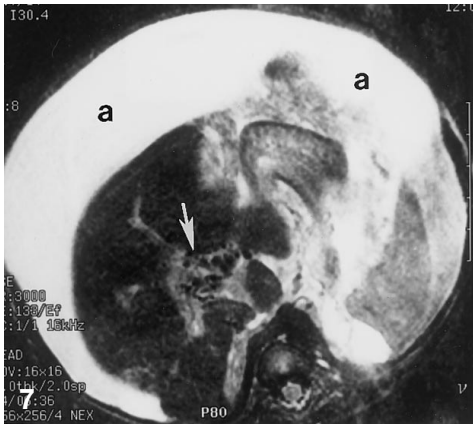

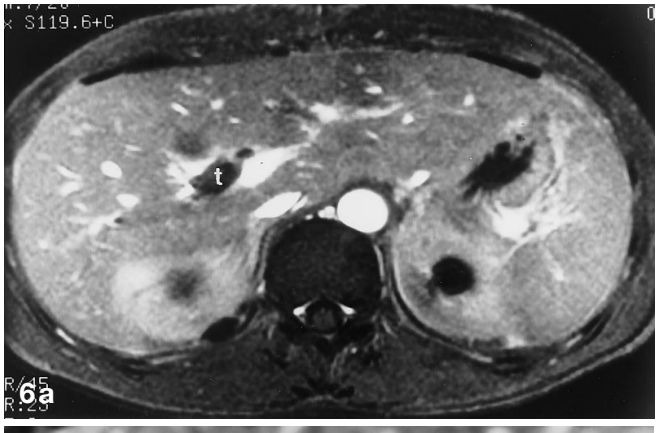

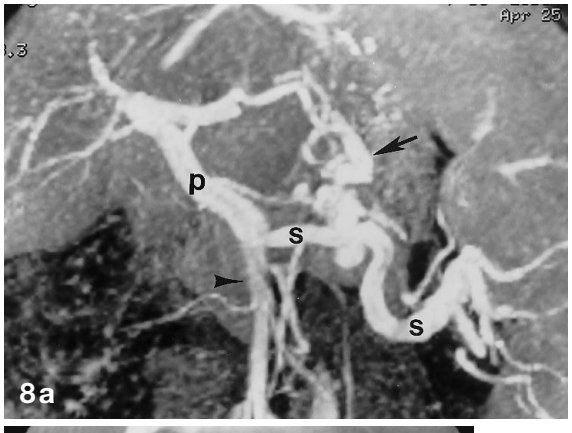

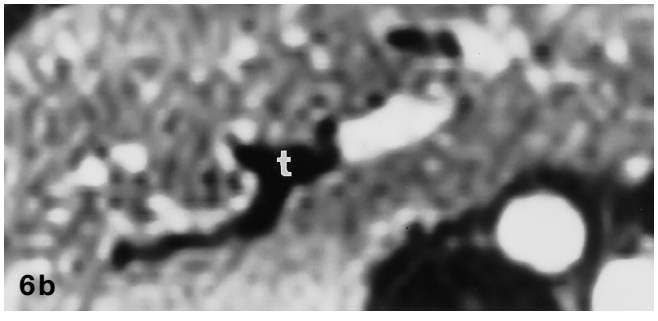

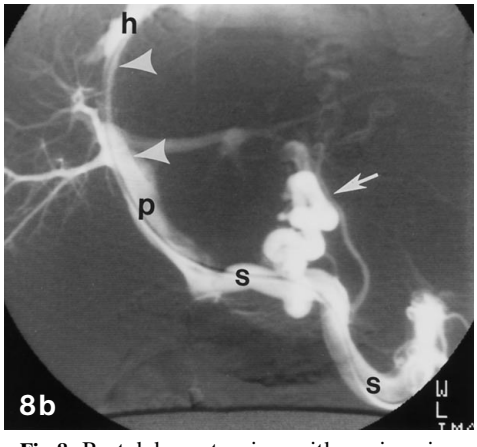

Fig. 5 A 2-year-old with hepatoblastoma extending into the inferior vena cava and right atrium (**a, b**). Black blood T1 spin echo coronal sections show the hepatoblastoma filling the IVC **a** and extending into the right atrium **b** *(arrows)*. Images obtained during mechanical ventilation in a previously intubated infant

Fig. 6 Non-occlusive acute portal vein thrombosis in an 18-year-old male with ulcerative colitis status-post ilioanal pull-through and with complaints of abdominal pain. **a** Axial 2D TOF image shows the right portal vein thrombosis *(t)*. Image obtained during quiet respiration. **b** 3D Gd MRA image in the axial plane shows the thrombosis *(t)*. Image obtained during breath-holding

Fig. 7 Cavernous transformation of the portal vein and venous collaterals in a 4-month-old with biliary atresia, post-Kasai operation with portal hypertension. Axial black blood T2-weighted image shows multiple small flow voids in the porta hepatis at the expected position of the portal vein, consistent with cavernous transformation *(white arrow)*. A large amount of ascites *(a)* is present. Images obtained during mechanical ventilation with the infant under general anesthesia for a subsequent interventional procedure

Fig. 8 Portal hypertension with varices in a 14-year-old female with autosomal recessive polycystic kidney disease. This condition is associated with hepatic fibrosis and the development of portal hypertension. The patient was imaged prior to a transjugular intrahepatic portosystemic shunt (TIPS) procedure to evaluate the patency of the portal vein. **a** Coronal 3D Gd MRA image demonstrates varices *(arrow)*. (*p* Portal vein, *s* splenic vein, *arrowhead* superior mesenteric vein). Images obtained during breath-holding in a child who had received anxiolytic medication. **b** Angiogram during the TIPS procedure demonstrates the same varices *(arrow)* (*h* hepatic vein, *arrowheads* TIPS shunt, *p* portal vein, *s* splenic vein)

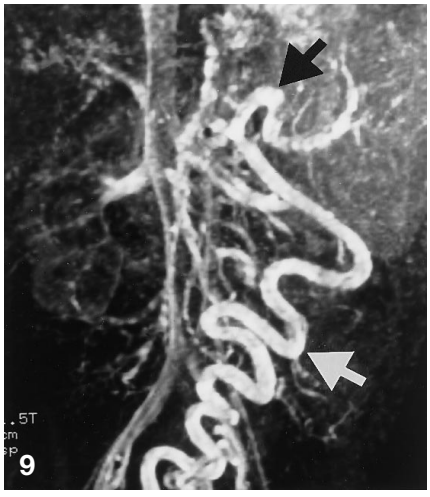

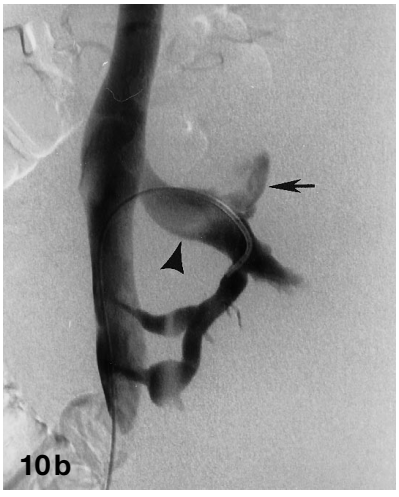

Fig. 9 Portal hypertension with a portosystemic collateral vein in an 8-month-old male with a history of tetralogy of Fallot repaired at 20 days of age. He developed upper gastrointestinal hemorrhage due to varices. The cause of the portal hypertension remains unknown. Coronal 3D Gd MRA image demonstrates a large, tortuous collateral *(white arrow)* arising from the splenic vein *(black arrow)* extending into the pelvis. Image obtained during quiet respiration with the child sedated

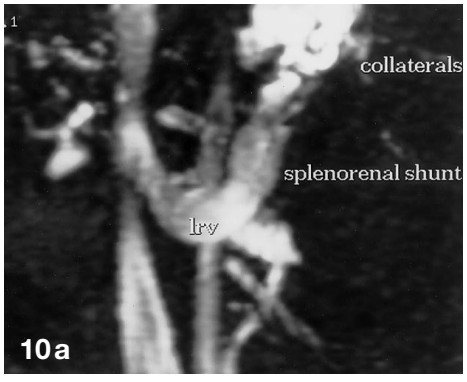

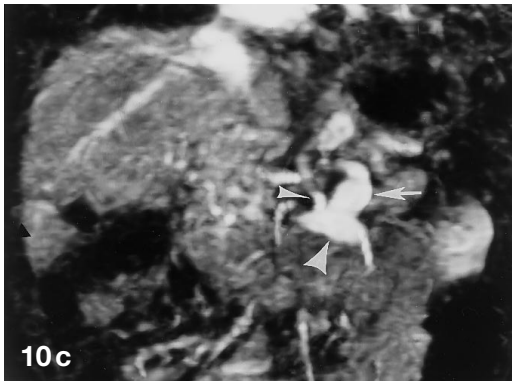

Fig. 10 Spontaneous and surgical spleno-renal shunts in a 5-year-old with idiopathic portal hypertension leading to the formation of a spontaneous splenorenal shunt. **a** Coronal MIP 2D TOF image shows the spontaneous spleno-renal shunt and collaterals. The portal vein was not visualized (*lrv* left renal vein). Images obtained during mechanical ventilation with the infant under general anesthesia for a subsequent interventional procedure. **b** Angiogram image with injection of contrast into the left renal vein *(arrowhead)* demonstrating reflux into the splenorenal shunt *(arrow)*. **c** Post-splenectomy with preservation of the spontaneous splenorenal shunt and the creation of a surgical splenorenal shunt. 3D Gd MRA image in the coronal plane shows both the surgical *(small arrowhead)* and spontaneous *(arrow)* shunts entering the left renal vein *(large arrowhead)*. Images obtained during suspended respiration with child under general anesthesia

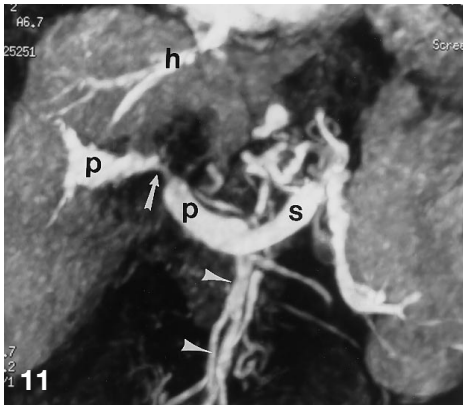

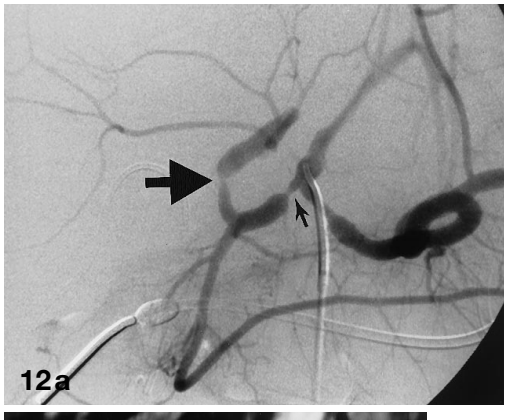

Fig. 11 Transplant portal vein stenosis in a 12-year-old boy. A 3D Gd MRA oblique coronal MIP image shows a focal portal vein stenosis *(arrow)*. Decreased signal at the liver hilum adjacent to the stenosis is due to post-transplant lymphoproliferative disorder (*arrowheads* superior mesenteric artery and vein, *h* hepatic vein, *p* portal vein, *s* splenic vein). Image obtained during breath-holding

Fig. 12 Post-liver transplantation arterial strictures in a 17-year-old female who presented with sudden onset of liver failure (same patient as Fig. 1). Investigations revealed a diagnosis of Wilson's disease and the patient underwent an orthotopic liver transplantation. When hepatic function failed to improve, an angiogram was performed revealing a stenosis of the common hepatic artery just distal to the celiac bifurcation. This stricture was angioplastied. **a** The preangioplasty arteriogram demonstrates the proximal common hepatic artery stenosis *(small arrow)*. In addition, there is a short focal stenosis of the proper hepatic artery at the arterial anastomosis *(large arrow)*. **b** 3D Gd MRA performed 4 weeks later shows both the proximal common hepatic artery stenosis *(small arrow)* and the more distal proper hepatic artery stenosis *(large arrow)*. Image obtained during breath-holding

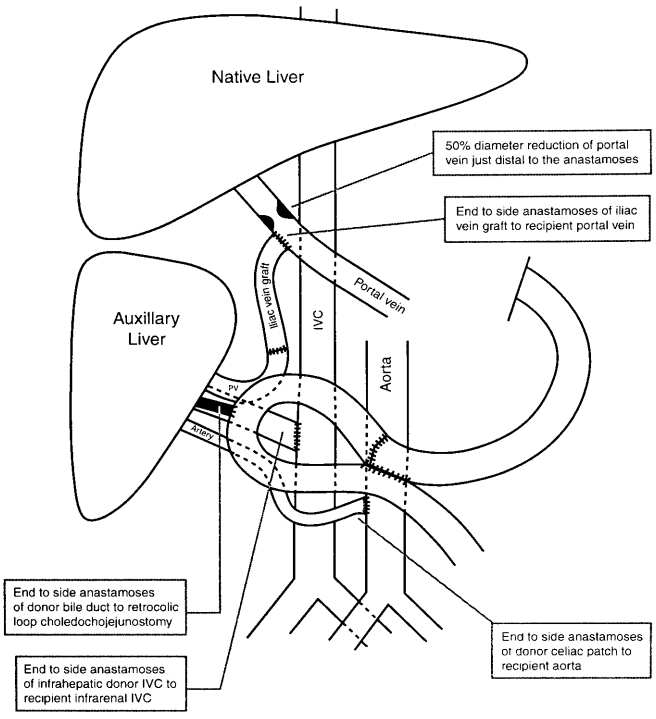

Fig. 13 Diagrammatic representation of auxiliary liver transplantation demonstrating vascular and bile duct anastomoses

MR techniques

Black blood MRI: spin echo sequences (Figs. 2–5, 7)

T1- and T2-weighted spin echo sequences produce flow or signal voids in vascular structures. Only protons that remain within the selected slice long enough to be exposed to both the initial 90° and the subsequent 180° radiofrequency pulse will emit a spin echo signal. Out-flowing and in-flowing blood that acquires only the 90° or the 180° pulse will emit no signal and therefore appear black.

White blood MRA: time-of-flight MRA (Figs. 6, 10)

In time-of-flight (TOF) MRA, short repetition times and rapidly repeated pulses saturate proton spins in stationary tissue, which cause them to appear dark [2]. Flowing blood that enters the imaging plane is not saturated, not having been exposed to the repeated pulses, and therefore appears bright. Consecutive thin slices are acquired individually. An advantage of the TOF technique is that images can be acquired in a relatively short time. TOF is extremely sensitive to slow blood flow. Disadvantages of TOF include poor spatial resolution and susceptibility to slice misregistration.

White blood MRA: 3D gadolinium enhanced MRA (Figs. 1, 6, 8–12, 14, 15)

3D gadolinium-enhanced (3D Gd) MRA is performed by injecting a sufficient dose (at least 0.2 mmol/kg) of gadolinium to make the T1 of blood shorter than the T1 of surrounding tissues, thereby making blood appear bright [3]. Images are obtained using a T1-weighted sequence such as a 3D spoiled gradient-echo pulse sequence. This sequence accentuates T1 contrast by suppressing signal from background tissue. Three-dimensional volume imaging provides high-resolution images, minimizes pulsatility artifacts and eliminates slice misregistration. Arterial phase images can be obtained by using a trigger mechanism, sensing the arrival of gadolinium in the aorta [4]. Venous phase images are obtained by repeating the acquisition or incorporating an appropriate delay. 3D Gd MRA is best interpreted on an independent computer workstation with 3D reconstruction capabilities. Analysis should always include scrutiny of the source images, thin multiplanar reformats of the underlying 3D data, as well as maximum intensity projection (MIP) images (Fig. 1) [3]. Although the 3D Gd MRA sequence is ideally performed with breath holding, interpretable images may be obtained with shallow respiration [1].

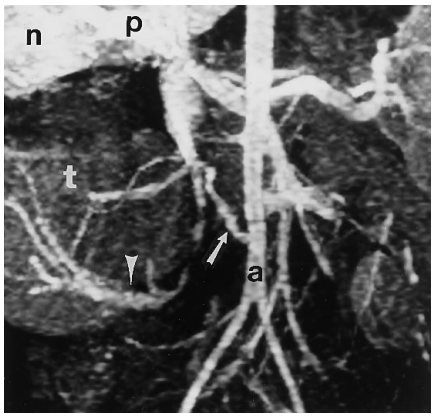

Fig. 14 Auxiliary liver transplant in a 6-year-old suffering from hepatic failure presumably due to halothane toxicity. Coronal 3D Gd MRA image shows the transplant hepatic artery *(white arrow)* originating from the aorta *(a)* (*n* native liver, *t* transplanted liver, *p* native portal vein, *arrowhead* transplant portal vein). Image obtained during suspended respiration in a previously intubated child

Case examples

For the assessment of congenital venous vascular anomalies (Fig. 2), hepatic tumor localization (Fig. 3), vascular supply (Fig. 4), and intravascular extension (Fig. 5), and acute or chronic portal vein thrombosis (Fig. 6, 7), T1-weighted black blood and TOF images are frequently adequate [5]. 3D Gd MRA is valuable in assessing portal vein patency and anatomy, particularly in older children, and in demonstrating collaterals (Figs. 6, 8, and 9) [6]. 3D Gd MRA is essential for the assessment of surgical splenorenal shunts (Fig. 10), with which small size and slow flow limit evaluation by other sequences.

MRA has a very important role in the assessment of the hepatic vasculature in pre- and post-liver transplant patients. Pre-transplant patients are initially assessed with sonography and Doppler. If an abnormality is identified, MRA can be performed for further evaluation. Studies have shown that portal venous patency, which is critical in patients awaiting liver transplantation, can

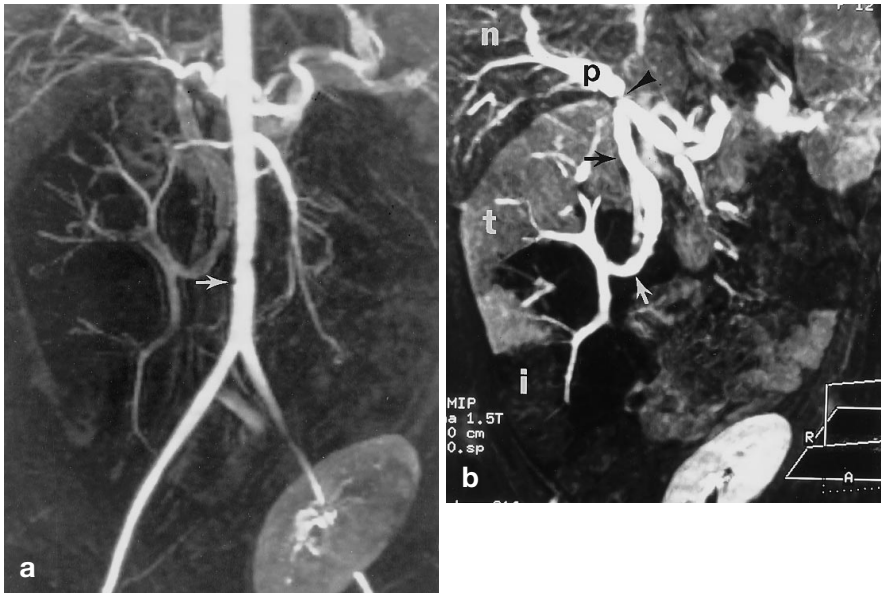

Fig. 15 Auxiliary liver transplant in a 12-year-old female suffering from methylmalonic aciduria. Coronal 3D Gd MRA images are shown. The arterial phase **a** shows occlusion of the transplant hepatic artery at its origin *(white arrow)*. A venous phase image **b** demonstrates the portal venous anatomy. The inferior-most aspect of the transplant liver *(t)* is infarcted *(i)*. Note the transplant kidney in the left lower quadrant (*n* native liver, *p* native portal vein, *black arrowhead* surgical portal vein stenosis, *black arrow* iliac vein graft, *white arrow* transplant portal vein). Images obtained with suspended respiration in a child under general anesthesia

be accurately assessed by MRA [7, 8]. 3D Gd MRA is valuable in assessing both the transplant hepatic artery and portal vein (Figs. 11, 12) [9]. Auxiliary liver transplantation is a form of liver transplantation in which the native liver is left in situ [10]. 3D Gd MRA delineates the complex anatomy (Figs. 13–15).

Discussion

MRI and MRA are valuable tools in the evaluation of many processes affecting the hepatic vasculature in pediatric patients. While non-invasive black blood MRI and TOF MRA sequences usually suffice to evaluate the portal vein and hepatic anatomy, 3D Gd MRA now allows for the assessment of smaller structures, including native and transplant hepatic arteries and surgical spleno-renal shunts. 3D Gd MRA is minimally invasive (intravenous access), can be utilized in both the sedated child and in the cooperative breath-holding child, and has become a powerful alternative to invasive angiography in the evaluation of pediatric liver disorders.

Acknowledgements The authors thank Bob Combs for photography and Judy Davids and Betty Reohr for their secretarial assistance. We also thank Betty Reohr for her artistic assistance (Fig. 13).

References

1. Lam WW, Chan JHM, Chan F (1998) Non-breath-hold gadolinium-enhanced MR angiography of the thoracoabdominal aorta: experience in 18 children. AJR 170: 478–480
2. Parker DL (1995) Time of flight magnetic resonance angiography. In: Yucel E (ed) Magnetic resonance angiography: a practical approach. McGraw-Hill, New York, pp 7–17
3. Prince MR, Grist TM, Debatin JF (1997) In: 3D contrast MR angiography. Springer, Berlin Heidelberg New York, pp 3–29
4. Prince MR, Chenevert TL, Foo TKF, et al (1997) Contrast enhanced abdominal MR angiography: optimization of imaging delay time by automating the detection of contrast material arrival in the aorta. Radiology 203: 109–114
5. Hughes LA, Hartnell GG, Finn JP, et al (1996) Time-of-flight MR angiography of the portal venous system: value compared with other imaging procedures. AJR 166: 375–378
6. Rodgers PM, Ward J, Baudouin CJ, et al (1994) Dynamic contrast-enhanced MR imaging of the portal venous system: comparison with X-ray angiography. Radiology 191: 741–745
7. Cheng YF, Huang TL, Lui CC, et al (1997) Magnetic resonance venography in potential pediatric liver transplant recipients. Clin Transplant 11: 121–126
8. Silverman JM, Podesta L, Villamil F, et al (1995) Portal vein patency in candidates for the liver transplantation: MR angiographic analysis. Radiology 197: 147–152
9. Stafford-Johnson DB, Hamilton BH, Dong Q, et al (1998) Vascular complications of liver transplantation. Evaluation with gadolinium-enhanced MR angiography. Radiology 207: 153–160
10. Heaton ND, Corbally MT, Rela M, et al (1995) Surgical techniques of segmental reduction, split and auxiliary liver transplantation. In: Williams R, Portmann B, Tan KC (eds) The practice of liver transplantation. Churchill Livingstone, New York, pp 140–149